Available online at www.sciencedirect.com
ScienceDirect
Applied Surface Science 253 (2007) 4361–4366
applied surface science
www.elsevier.com/locate/apsusc

# Electron beam-physical vapor deposition of $SiC/SiO_2$ high emissivity thin film

Jian Yi *, XiaoDong He, Yue Sun, Yao Li

*Center for Composite Materials, Harbin Institute of Technology, P.O. Box 3010, Harbin 150001, PR China*

Received 30 May 2006; received in revised form 22 September 2006; accepted 22 September 2006
Available online 25 October 2006

**Abstract**

When heated by high-energy electron beam (EB), SiC can decompose into C and Si vapor. Subsequently, Si vapor reacts with metal oxide thin film on substrate surface and formats dense $SiO_2$ thin film at high substrate temperature. By means of the two reactions, $SiC/SiO_2$ composite thin film was prepared on the pre-oxidized 316 stainless steel (SS) substrate by electron beam-physical vapor deposition (EB-PVD) only using β-SiC target at 1000 °C. The thin film was examined by energy dispersive spectroscopy (EDS), grazing incidence X-ray asymmetry diffraction (GIAXD), scanning electron microscopy (SEM), atomic force microscopy (AFM), backscattered electron image (BSE), electron probe microanalysis (EPMA), X-ray photoelectron spectroscopy (XPS) and Fourier transformed infra-red (FT-IR) spectroscopy. The analysis results show that the thin film is mainly composed of imperfect nano-crystalline phases of 3C-SiC and $SiO_2$, especially, $SiO_2$ phase is nearly amorphous. Moreover, the smooth and dense thin film surface consists of nano-sized particles, and the interface between $SiC/SiO_2$ composite thin film and SS substrate is perfect. At last, the emissivity of SS substrate is improved by the $SiC/SiO_2$ composite thin film.


*Keywords:* EB-PVD; SiC; $SiO_2$; High emissivity; Thermal protection

## 1. Introduction

Metal thermal protection systems (MTPS) widely used in third generation reused space vehicles are usually in the form of rigid surfaces in areas of moderate working temperature [1]. High friction heat from acute friction between space vehicle surface and atmosphere causes severe increase of surface temperature during hypervelocity flights and affects the life of reused space vehicle. Furthermore, elevated temperature and high heat fluxes demand TPS materials must be endowed with good oxidation and thermal shock resistance, dimensional stability and ablation resistance [1]. To improve the multi-mission lifecycle of MTPS, a multifunctional thermal protection coating can be used in MTPS. The applied thermal protection coating must protect MTPS from high temperature and ablation of hypervelocity particles as maximum as possible. Moreover, the applied thermal protection coating must be endowed with good oxidation, thermal shock and corrosion resistance.

SiC is a promising multi-function protective coating material for MTPS because of their combination of unique physicochemical and mechanical properties in rigid condition, such as ultra high velocity and temperature condition [2–5]. Besides the excellent resistance to elevated temperature, oxidation, corrosion and ray radiation, SiC also possess the properties of high hardness, low friction coefficient and high emissivity. Furthermore, because of low thermal conductivity and high oxidation resistance, $SiO_2$ can act as an additive oxidation insulator layer between SiC thin film and MTPS to increase oxidation resistance of MTPS [6–8]. When reusable space vehicle hypervelocity flying, surface temperature of the section using $SiC/SiO_2$ coating mainly comes from friction between air flow and vehicle surface. One hand, $SiC/SiO_2$ coating of low friction factor reduces surface friction heat. On the other hand, high emissivity can make $SiC/SiO_2$ coating radiate a quantity of thermal energy to atmosphere, and reduce surface temperature of space vehicle and inward heat transfer.

In the present work, $SiC/SiO_2$ composite thin film was successfully deposited on the pre-oxidized 316 SS substrate by EB-PVD only using β-SiC target at 1000 °C, and characterized subsequently.

* Corresponding author. Tel.: +86 451 8640 2345; fax: +86 451 8640 2345.
*E-mail address:* yj_hit@163.com (J. Yi).

0169-4332/$ – see front matter © 2006 Elsevier B.V. All rights reserved.
doi:10.1016/j.apsusc.2006.09.063

## 2. Experimental

SiC thin film was deposited on the 316 SS substrate by EB-PVD. Ultra fine 3C-SiC powder, with the average particle size of approximately 0.3 μm, was sintered into ingot of 68.5 mm in diameter and 100 mm in length in vacuum. Before SiC ingot was filled in a water-cooled crucible, SiC ingot has been dried at 300 °C for 12 h in vacuum chamber. The 316 SS substrate surface was pre-oxidized. The substrate temperature was kept at 1000 °C, the distance between target and substrate was 150 mm, and the pressure of vacuum chamber was maintained at $9.0 \times 10^{-3}$ Pa during deposition. In the initial stage of evaporation, EB was used with high current intensity to obtain Si vapor. Subsequently, EB was reduced to a low value to obtain perfect SiC vapor.

The crystallization and composition of the film was studied by EDS and GIAXD with Cu Kα radiation under incidence angle of 3°. The morphology of the film surface was examined by SEM and AFM. The morphology of cross-section of the film was examined by BSE. The composition across thin film cross-section was determined by EPMA. XPS spectroscopy was carried out using Al Kα radiation at 1486.6 eV. Infrared spectra were recorded on a FT-IR spectrometer with incident angle of 30° (between 400 and 2000 $cm^{-1}$) and 80° (between 400 and 4000 $cm^{-1}$) in reflection. A gold mirror on glass was used as reference sample.

## 3. Results and discussion

### 3.1. Reaction mechanism

When heated by EB of high current intensity, SiC can decompose into C and Si elements. At the same time, because saturated vapor pressure of Si is larger than that of C and SiC, decomposed Si will firstly reach and react with metal oxide ($Me_2O_3$) thin film on the substrate at high substrate temperature. The two reactions are expressed as follows:

$$SiC \rightarrow C + Si \quad (1)$$

$$Si + Me_2O_3 \rightarrow Me_2O + SiO_2 \quad (2)$$

Based on the two reactions, $SiC/SiO_2$ composite thin film was prepared on the pre-oxidized 316 SS substrate by EB-PVD only using β-SiC target at 1000 °C.

### 3.2. Composition and crystalline

Fig. 1 shows GIAXD pattern of the composite thin film deposited by EB-PVD at 1000 °C. From Fig. 1, it can be shown that the film is mainly composed of 3C-SiC and a small mount of $SiO_2$, which are both imperfect crystalline phases. Especially, $SiO_2$ in the film is nearly amorphous. Moreover, the 3C-SiC (1 1 1) reflex shifts slightly to lower angle (35.575°) than that of the reference data [9], which caused by thin nanocrystal and residual stress in the composite thin film.

The EDS microanalysis (Fig. 2) of the film surface reveals that the film includes elements of Si, C and O, and the Si peak is the highest, as illustrated in Fig. 3(b). However, peaks of C and O elements are quite low because they are low-Z elements and there are large measurement errors in the EDS microanalysis.

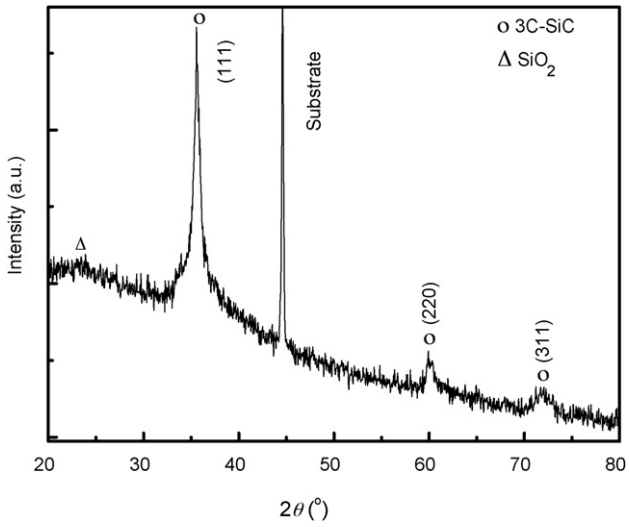


Fig. 1. GIAXD pattern of $SiC/SiO_2$ composite thin film prepared by EB-PVD at 1030 °C.

### 3.3. Surface chemistry analysis

The XPS of C 1s core level photoelectron binding energy (BE) of the prepared sample is shown in Fig. 3(a). Curve 1 shows spectrum of the as-deposited sample and curve 2 is the spectrum obtained after Ar sputtering at 1 kV accelerating voltage for 2 min. After sputtered for 2 min, there is only one peak representing C–Si existing in curve 2 and peak representing C–C existing in curve 1 nearly vanished. On the other hand, it can also be seen that there is a widening and shifts toward higher binding energy of the peak representing C–Si in comparison with that in curve 1. Moreover, the binding energy of C–Si (283 eV) in curve 2 is very close to that of single-crystalline 3C-SiC [10]. All of above reveal that C–Si

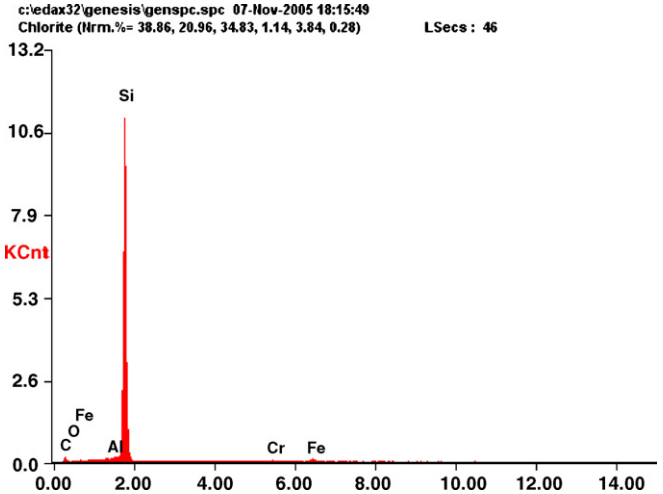


Fig. 2. EDS microanalysis of $SiC/SiO_2$ composite thin film prepared by EB-PVD at 1030 °C.

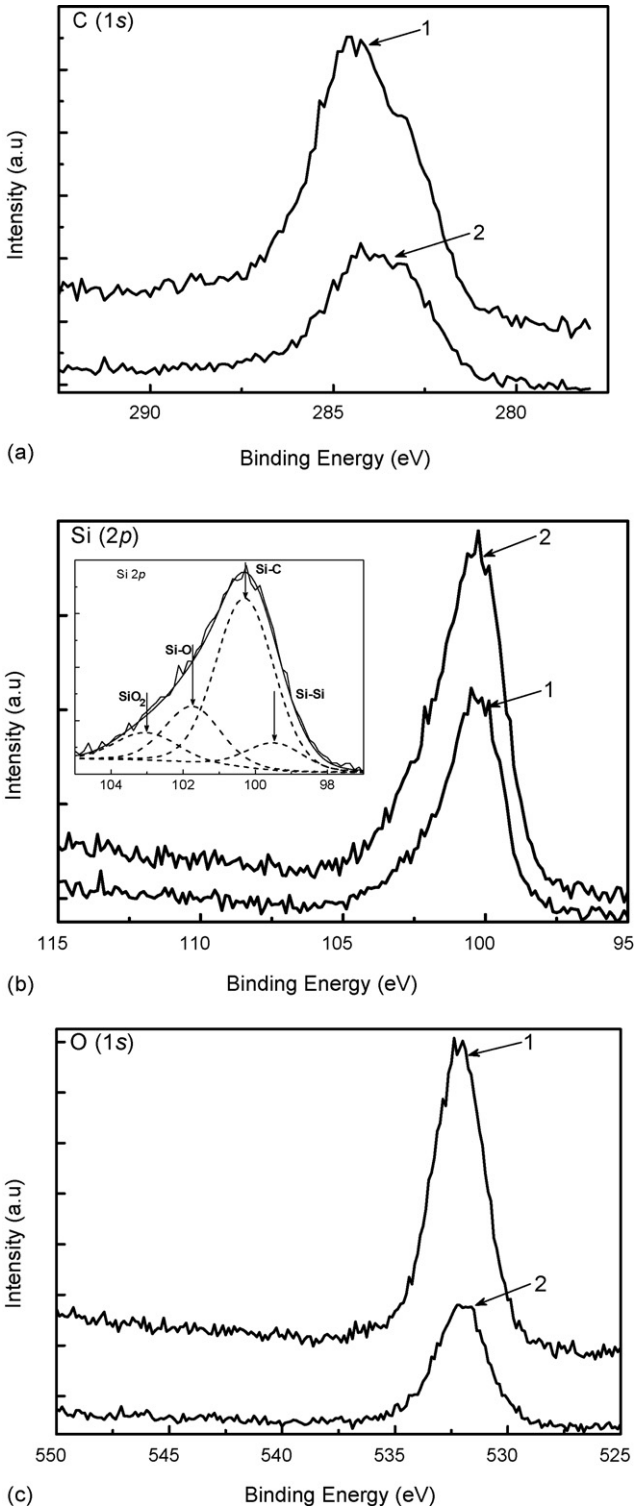


Fig. 3. XPS spectra of as-deposited EB-PVD sample (curve 1) and after Ar sputtering (curve 2). (a) C 1s spectrum, (b) Si 2p spectrum and (c) O 1s spectrum. The inset in (b) shows deconvolution of Si 2p XPS spectrum.

bond in the film is possibly attribute to 3C-SiC prepared by EB-PVD, and the experimental peak representing C–C in as-deposited sample is attributed to adventitious carbon (i.e., C bonded with four carbon atoms (C–C) in graphite).

Inconsistent with the XPS of C 1s, there are a narrowing at the bottom, widening at the top and shift toward lower binding energy of the Si 2p core level spectrum [Fig. 3(b)] of sample sputtered for 2 min (curve 2) in comparison with that of as-deposited sample (curve 1). The Si 2p Peak at 100.1 eV in curve 2 is due to the Si–C bond in 3C-SiC and is in fairly good agreement with similar XPS peaks in spectra of powder [11], whisker [10] and single crystal [10]. According to Pivac et al. [12] the shoulder peak in curve 2 (100.5 eV) is also attribute to Si–C bond, and the high binding energy tail is indicative of the $SiO_x$ species in the film. The inset in Fig. 3(b) is the deconvolution of Si 2p XPS spectrum, which shows that the peak occurring at 103 eV is related to $SiO_2$ according to Hollinger and Himpsel [13]. Moreover, the peak at 101.7 eV can be attributed to Si bonded to O.

Fig. 3(c) shows the XPS of O 1s core level spectrum in as-deposited (curve 1) and sputtered for 2 min (curve 2) sample. The O 1s peak (532 eV) in sample sputtered for 2 min unambiguously reveals a drastically decrease and shift toward lower binding energy compared to that (533 eV) in as-deposited sample. According to Avila et al. [14] the O 1s peak in curve 1 is attributed to O–Si, and the O 1s peak in curve 2 is attributed to Si–O–C or SiC:O. On the other hand, the spectra of the composite film are dominated by $SiO_2$ signal. It is noteworthy that the carbon-to-oxygen-to-silicon concentration ratio in sample deduced from the peak areas and corrected by the atomic sensitivity factor changed from 1.8:1:0.5 in as-deposited sample into 2:1:1.4 in sample sputtered for 2 min. Which indicates that there is excess C existing at the surface of thin film, i.e., C appears as graphite (C–C) and polymeric ($C–C_{4-n}Si_n$, $n = 1–4$) components [15], and Si occurs with Si–C bond and Si–O bond. Furthermore, the loss of Si in film can be relative with secondary sputtering and infiltration into substrate. The XPS data of C 1s, Si 2p, and O 1s spectra are consistent with the result of GIAXD (Fig. 1), and demonstrated by the results of EPMA (Fig. 6).

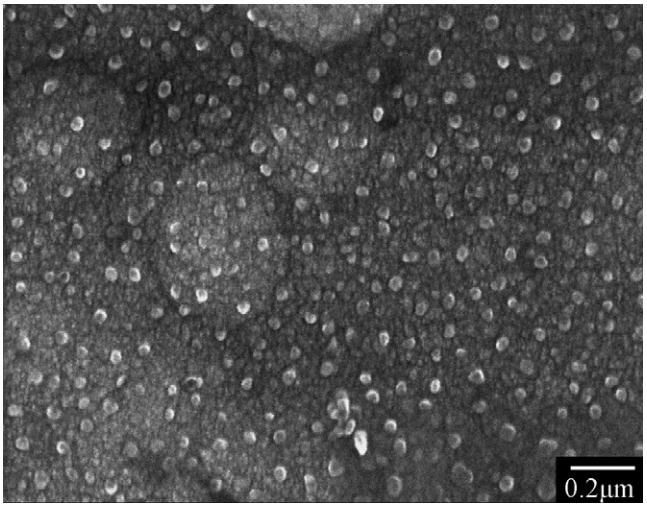


Fig. 4. SEM image of $SiC/SiO_2$ composite thin film prepared by EB-PVD at 1000 °C.

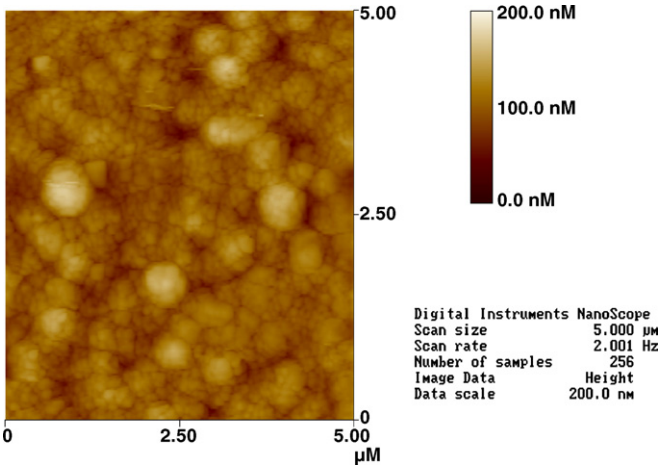


Fig. 5. Top-view AFM image of $SiC/SiO_2$ composite thin film prepared by EB-PVD at 1000 °C.

### 3.4. Surface morphology

The surface morphology of the film was examined by SEM image (Fig. 4) and AFM image (Fig. 5). Fig. 4 shows a smooth and dense surface consisting of nano-sized particles, and the largest particle is no more than 50 nm. Moreover, there are lots of cauliflower-like crystal clusters, which caused by crystals agglomeration at three dimensional island growth mode of the film. In particular, it does not exhibit any features that can be clearly attributed to cracks. Fig. 5 shows AFM image in contact mode for the film. Smooth and dense surface morphology is evident. The root mean square (r.m.s.) roughness of 17 nm was evaluated from 25 $\mu m^2$ surface area.

### 3.5. Cross-section measurement

From the BSE and line profiles across section of the film (Fig. 6), the thickness and the growth rate of the film can be measured. The results are approximately 0.5 μm and 1 μm/min, respectively. Moreover, it can be shown that the unambiguous interpenetration of C, Si, O, Fe, etc. elements occurred at the interface between the film and SS substrate. Although it's not explicit that if elements of the film reacted with that of SS substrate, it is possible to deposit thin films with composition gradients of the components by EB-PVD, which is very interesting for improving the adhesion between the film and substrate. Furthermore, O element concentration abruptly has a maximum at the interface between the film and SS substrate, which indicates that $SiO_2$ formed around the interface between the film and SS substrate.

Before examined by electron probe microanalysis (EPMA), the specimens with $SiC/SiO_2$ coatings had been longitudinally inlayed in phenolic moulding powder (contains a large quantity of C) and make into cylindrical samples. In addition, beam spot diameter of EPMA probe is approximate 1 μm, however, the thickness of $SiC/SiO_2$ coating is only about 0.5 μm, which leads to a rather larger error during inspecting the content distribution of C and Fe (represents composites of substrate)

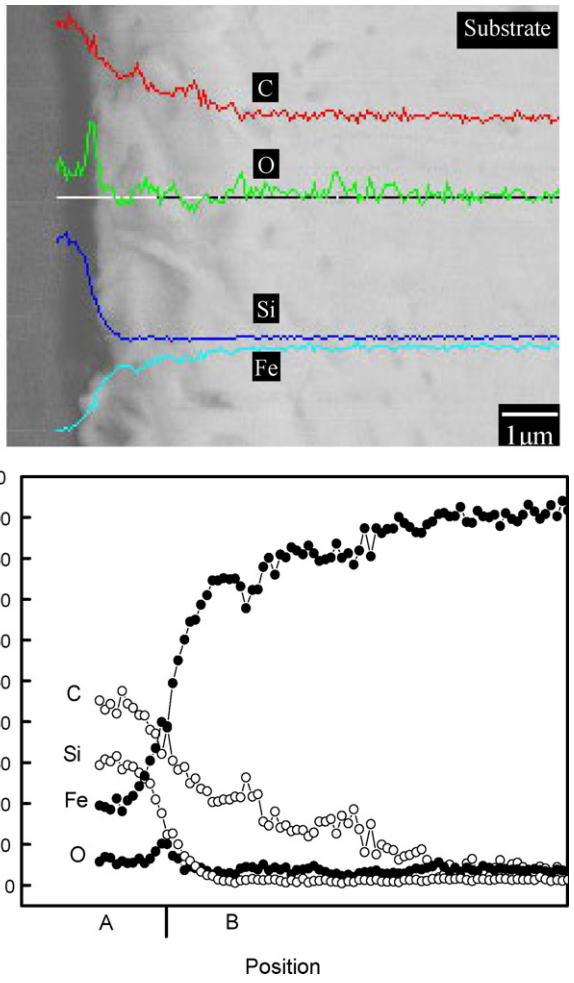


Fig. 6. Cross-sectional micrograph along with elemental distribution across the thickness of $SiC/SiO_2$ composite thin film. (A) Film and (B) substrate.

from coating to substrate. So EPMA is only used for qualitative reflecting the compositions distribution tendency along the interface between coating and substrate. Because saturated vapor pressure of Si element is much higher than SiC and C, which firstly reach substrate and should has a high concentration at the interface. However, concentration of Si is higher at the middle of thin film, and gradually reduces from middle to two edges of thin film. One possible interpretation is that severe secondary sputtering occurs when Si element reach SS substrate, especially in the initial stage of deposition, which results in a great deal of loss of Si, as can be demonstrated by line profiles across section of Si (shown in Fig. 6).

### 3.6. Emissivity and optical properties

The hemisphere integrated (spatial) direction emissivity of $SiC/SiO_2$ composite thin film is about 0.29 measured at 423 K by the radiation heat-equilibrium method (filament method), with a wave length range from 2 to 18 μm. At the same experiment condition, the spatial direction emissivity is 0.22. Which shows that spatial direction thermal emissivity of 316 SS by depositing $SiC/SiO_2$ composite thin film on it's surface. In

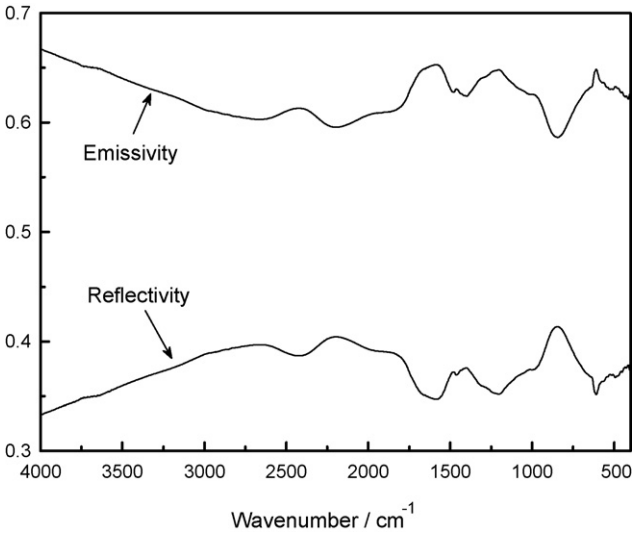


Fig. 7. The emissivity and reflectivity of $SiC/SiO_2$ composite thin film as a function of wavenumber.

addition, the reflectance of $SiC/SiO_2$ composite thin film was also inspected by FT-IR. Due to $A = 1 - R - T$ ($A$, absorptivity; $R$, reflectivity; $T$, transmissivity), in the limit of strong absorption ($T = 0$), according to Kirchhoff's law, the emittance is determined by the first surface reflection, such that:

$$\varepsilon(\nu, T, \theta) = 1 - R(\nu, T, \theta) \quad (3)$$

where $\varepsilon$ is the emissivity, $\nu$ the frequency, and the angle $\theta$ specifies the observer angle. As shown in Fig. 7. Because there is no transmittance, the reflectance equals the single surface power reflection coefficient. According to Andersson and Thomas [16], when $n - 1 \gg k > 0.01$ ($n$ and $k$: the real and imaginary parts of the complex index of refraction), the spectral region occurs in the two-phonon region (shown in Fig. 8), which is the spectral region of highest emissivity for a bulk material. Corresponding with bulk material, the $SiC/SiO_2$ composite thin film also has a highest emissivity in this spectral region. Because the emissivity fluctuates at 0.65, the $SiC/SiO_2$ composite thin film has a stable spectral direction emissivity at a wide wave-number range from 400 to 4000 ($cm^{-1}$). Of course, it isn't quite precise that reflectivity of $SiC/SiO_2$ composite thin film is measured with a incident angle of 80°, which results in a part of light absorbed in the progress of FT-IR experiment. The real reflectivity of $SiC/SiO_2$ composite thin film will be a little higher than the result of FT-IR experiment.

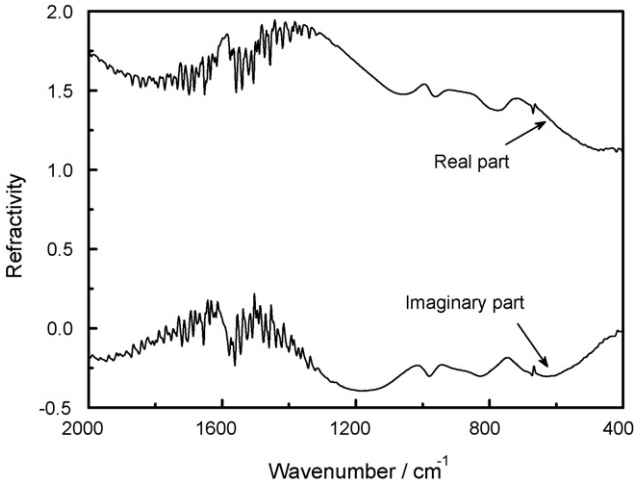


Fig. 8. The real and imaginary parts of refractivity of $SiC/SiO_2$ composite thin film as a function of wavenumber.

## 4. Conclusion

$SiC/SiO_2$ composite thin film with the thickness of 0.5 μm was successfully deposited on SS substrate by EB-PVD only using β-SiC target at 1000 °C. The composite thin film is main composed of imperfect crystalline phase of 3C-SiC and a small mount nearly amorphous phase of $SiO_2$. However, C:Si is nearly 2:1.4 other than 1:1 at the surface of thin film, there is excess C at the surface of thin film. The thin film surface is smooth and consists of nano-sized particles. And the unambiguous interpenetration of C, Si, O, Fe etc. elements occurred at the interface between the film and SS substrate, which indicates that the bond strength between thin film and substrate is perfect. Moreover, because severe secondary sputtering occurs when Si element reach SS substrate, especially in the initial stage of deposition, concentration of Si is higher at the middle of thin film, and gradually reduces from middle to two edges of thin film.

The deposited $SiC/SiO_2$ composite thin film with a spatial emissivity of 0.29 improves spatial emissivity of SS substrate surface. At the same time, the emissivity of $SiC/SiO_2$ composite thin film minorly lightly fluctuates and has a stable spectral direction emissivity at the range from 400 to 4000 ($cm^{-1}$). At last, all the above demonstrate that EB-PVD is a suitable technology to prepare $SiC/SiO_2$ composite thin film.

## Acknowledgement

This project was supported by the New Century Excellent Talents Plan of China (NCET2004).

## References

[1] C. Bartuli, T. Valente, M. Tului, Surf. Coat. Technol. 155 (2002) 260.
[2] A. Ordine, C.A. Achete, O.R. Mattosa, I.C.P. Margarit, S.S. Camargo Jr., T. Hirsch, Surf. Coat. Technol. 133–134 (2000) 583.
[3] S. Ulrich, T. Theel, J. Schwan, V. Batori, M. Scheib, H. Ehrhardt, Diam. Relat. Mater. 6 (1997) 645.
[4] S.K. Gong, H.B. Xu, Q.H. Yu, C.G. Zhou, Surf. Coat. Technol. 130 (2000) 128.
[5] A.K. Costa, S.S. Camargo Jr., C.A. Achete, R. Carius, Thin Solid Films 377–378 (2000) 243.
[6] Z.Q. Fu, C.H. Tang, T.X. Liang, R.J. Charles, Nucl. Eng. Des. 234 (2004) 45.
[7] H. Kobayashi, T. Sakurai, M. Takahashi, Y. Nishioka, Phys. Rev. B 67 (2003) 115305.
[8] G.V. Soaresa, C. Radtke, I.J.R. Baumvol, F.C. Stedile, Appl. Phys. Lett. 88 (2006) 041901.

[9] Interantional Centre for Diffraction Data reference cards No. 29-1129.
[10] K. Miyoshi, D.H. Buckley, Appl. Surf. Sci. 10 (1982) 357.
[11] T.N. Taylor, J. Mater. Res. 4 (1989) 189.
[12] B. Pivac, K. Furic, M. Milun, T. Valla, A. Borghesi, A. Sassella, J. Appl. Phys. 75 (1994) 3586.
[13] G. Hollinger, F.J. Himpsel, Appl. Phys. Lett. 44 (1984) 93.
[14] A. Avila, I. Montero, L. Galán, J.M. Ripalda, R. Levy, J. Appl. Phys. 89 (2001) 212.
[15] K. Mui, F.W. Smith, Phys. Rev. B 35 (1987) 8080.
[16] S.K. Andersson, M.E. Thomas, Infra. Phys. Technol. 39 (1998) 223.